Brønsted Ionic Liquids for Sustainable Processes: Synthesis and Physical Properties[†]

Víctor H. Álvarez,[‡,§] Noelia Dosil,[‡] Rebeca Gonzalez-Cabaleiro,[‡] Silvana Mattedi,[||] Manuel Martin-Pastor,[⊥] Miguel Iglesias,*[,‡] and José M. Navaza[‡]

Chemical Engineering Department - ETSE, University of Santiago de Compostela, P.O. Box 15782, Santiago de Compostela, Spain, School of Chemical Engineering, State University of Campinas, P.O. Box 6066, 13083-970 Campinas-SP, Brazil, Chemical Engineering Department, Polytechnic School, Federal University of Bahia, 40210-630 Salvador-BA, Brazil, and Unidade de Resonancia Magnética, RIAIDT, edif. CACTUS, University of Santiago de Compostela, P.O. Box 15706, Santiago de Compostela, Spain

This report describes the synthesis of ionic liquids that incorporate the *N*-methyl-2-hydroxyethylammonium cation with various carboxylic acid anions and the study of some of their physical properties, including self-diffusion coefficients, density, speed of sound, viscosity, and refractive index. ^{1}H and ^{13}C NMR spectra were used to characterize the chemical structure of the species in concordance with FT-IR spectra. DOSY NMR spectra was used to determine the self-diffusion coefficients of the components, which were consistent with the formation of a lamellar or micellar liquid-crystal phase in samples containing an alkyl chain in the anion species. Thermoacoustic parameters showed that anion alkyl chain has an influence on the molecular packing of these ionic liquids. In addition, the effect of temperature on the properties seems to be related to the size and the type of aliphatic chain of the ionic liquid.

Introduction

Ionic liquids (ILs) are versatile new media for many chemical synthesis, enzymatic catalysis, and green engineering processes. ILs consist solely of a collection of positive and negative ions of hydrophobic or hydrophilic nature. However, unlike conventional molten salts, these materials often melt below 373 K. This is achieved because the ion-pair packing prevents an ordered electrostatic net structure as a result of steric hindrance, and therefore, a solid phase cannot form under ambient conditions.

ILs can be used as solvents because of their low melting points and their ionic structure. In some cases where ILs are used as solvents, better selectivity for organic reactions or molecular absorption is obtained than with conventional organic solvents because of specific interactions among the ions. In the past few years, room-temperature ILs have found a number of applications as clean solvents and catalysts for green chemistry, as electrolytes for batteries, in photochemistry, for electrosynthesis,[1−5] and others.

One of the properties of ILs of interest for chemistry is their negligible vapor pressure, which means that no volatile organic pollution is created during their manipulation in industrial operations. Their liquid range can be as large as 300 °C, allowing for large reaction kinetic control and easy separation of organic molecules by distillation without loss of the IL. Until now, many ILs have been based on the imidazolium cation and, in a lesser proportion, on alkylpyridinium cations and trialkylamines.[6] By variation of the anion or the alkyl chain of the cation, a wide range of properties such as hydrophobicity, viscosity, density, and solvation power can be modulated, opening the possibility of tailored ILs designed for specific industrial applications.[7] In this way, Bicak[8] synthesized an IL formed from the neutralization of monoethanolamine with formic acid. Greaves et al.[9] proposed different protic ILs obtained from primary amines and organic and inorganic acids. Iglesias and co-workers[10−12] synthesized a family of these ILs by modifying the aliphatic chain of the organic acid and/or using secondary and tertiary hydroxylamines. These authors explained the low cost, simplicity of synthesis, and different applications of this new IL family. Moreover, the very low toxicity and the degradability of this kind of IL was verified.[13] Thus, sustainable processes can be originated with their use. Therefore, available physicochemical properties or a thermodynamic database for this class of IL, either pure or in mixtures, can be of technological and/or theoretical interest.

Structural and physicochemical properties of ILs can be studied with conventional liquid NMR methods.[14] These techniques can be useful in assessing the chemical composition of the ILs and for quantitative analysis of the species. In addition, NMR diffusion-ordered spectroscopy (DOSY) experiments can be used to determine self-diffusion coefficients, which are related to the molecular size and viscosity of these samples.

Continuing with our previous studies, this paper presents the synthesis and study of a series of physicochemical properties of ammonium-based ILs. We present the synthesis of six ILs, *N*-methyl-2-hydroxyethylammonium formate (m-2-HEAF), *N*-methyl-2-hydroxyethylammonium acetate (m-2-HEAA), *N*-methyl-2-hydroxyethylammonium propionate (m-2-HEAPr), *N*-methyl-2-hydroxyethylammonium butyrate (m-2-HEAB), *N*-methyl-2-hydroxyethylammonium isobutyrate (m-2-HEAiB), and *N*-methyl-2-hydroxyethylammonium pentanoate (m-2-HEAP). For these ILs, the following physicochemical properties were studied: density (ρ), speed of sound (u), refractive index (n_D), apparent viscosity (η), and self-diffusion coefficient (D).

[†] Part of the "2009 Iberian Conference on Ionic Liquids".
* Corresponding author. E-mail: miguel.iglesias@usc.es.
[‡] Chemical Engineering Department, University of Santiago de Compostela.
[§] State University of Campinas.
[||] Federal University of Bahia.
[⊥] Unidade de Resonancia Magnética, University of Santiago de Compostela.

10.1021/je900550v
Published on Web 01/08/2010

Experimental Section

Materials and Methods. 2-(Methylamino)ethanol (mass fraction purity 0.99) was obtained from Aldrich, and the organic acid (mass fraction purity 0.995) was obtained from Sigma. These components were used as received, as the water content (< 0.5 %) could be removed after the synthesis. During the course of the experiments, the purity of the solvents was monitored by the density and the speed of sound measurements.

The densities and the speeds of sound of the pure liquids were measured using a DSA-5000 digital vibrating tube densimeter (Anton Paar, Austria). This apparatus performs an automatic viscosity correction when used with high-viscosity liquids. The accuracy is ± 0.01 K for temperature, and the uncertainty is ± $1 \cdot 10^{-4}$ g·cm^{-3} for the density measurement and ± 0.1 m·s^{-1} for the speed of sound, as calculated by propagation of errors. Dry air and distilled water were used as reference fluids to calibrate the densimeter at each temperature. The mass of each component was determined on a Kern 770 mass balance having an accuracy of 0.0001 g. The apparent viscosities of IL samples were analyzed using a Visco Elite L rheometer (Fungilab, Spain) at different temperatures. The spindles used were the TL5, TL6, and TL7, and the speed ranges were selected in accordance with the torque range (minimum 10 % and maximum 90 %), as suggested by the manufacturer's instructions. The temperature was controlled with a thermostatic bath and measured with a calibrated thermometer close to the jacket of the viscosimeter. The refractive indexes of the ILs were analyzed by an automatic digital RX-5000 refractometer (Atago, Japan). The temperature was controlled with a thermostatic bath and measured with a PT 100 sensor provided in the refractometer that had a precision of ± 0.1 K for the temperature measurement. The thermostatic bath used was the Frigiterm equipment (J.P. Selecta S.A., Spain) with a temperature stability of ± 0.1 K.

Each refractive index was obtained as the mean of three measurements with a standard deviation of $2 \cdot 10^{-5}$, and the apparent viscosity was obtained as the mean of five different spindle rate measurements with a standard deviation of 0.5 mPa·s at temperatures from (308 to 323) K and 4.0 mPa·s at temperatures from (288 to 303) K.

FT-IR Spectroscopy. The FT-IR spectra were obtained with a Varian FT-IR 670 spectrometer set to acquire the medium- and high-IR-range spectrum [(7900 to 20) cm^{-1}]. The device has a resolution of 0.10 cm^{-1} and a signal-to-noise ratio of 12 000:1 with 75 % light attenuation. The ATR method was used for the synthesized ILs, and the sample film for these measurements was formed using a drop of IL.

NMR Spectroscopy. All of the NMR experiments were performed at 298 K in an 11.7 T Varian Inova-750 spectrometer operating at 750 MHz proton frequency. The spectra were processed with Mestre-C software.[15]

Samples of m-2-HEAF, m-2-HEAA, m-2-HEAPR, m-2-HEAB, m-2-HEAiB, and m-2-HEAP were studied by NMR spectroscopy. Sample preparation required only the transfer to a 5 mm NMR tube. An external reference standard capillary containing deuterated 3-(trimethylsilyl)propionic acid-d_4 (TSP) [0.1 M in dimethyl sulfoxide (DMSO)] was introduced coaxially in the tube. The TSP signal at approximately 0 ppm was used to determine absolute concentrations in the one-dimensional (1D) proton spectrum, and the DMSO was used for deuterium lock. The integral of the ^{1}H NMR signal of TSP in the capillary was calibrated with respect to a sample of 0.2 M sucrose dissolved in D_2O prepared in a 5 mm NMR tube. The anomeric glucose proton appearing at 5.2 ppm was chosen for the calibration.

The following NMR experiments were acquired for each sample:

A quantitative 1D ^{1}H NMR experiment was acquired with a 33° pulse and a conveniently long interscan relaxation time (d_1 = 10 s). These conditions were used to ensure the exactness of the signal integration.

1D ^{13}C, 1D ^{15}N, 2D total correlation spectroscopy (TOCSY), 2D heteronuclear multiple-quantum coherence (HMQC), and 2D heteronuclear multiple-bond quantum coherence (HMBC) NMR spectra were acquired using standard methodologies.

NMR DOSY experiments were measured with the convection-compensated double-stimulated echo sequence.[16] Diffusion encoding and decoding periods were done with pulsed-field bipolar gradients, and the duration of a pair of bipolar gradients was 4 ms. The gradient power level (G in eqs 1 and 2) used for diffusion encoding/decoding was varied linearly between (2 and 62) G·cm^{-1} in 50 steps, with acquisition of the free-induction decay at each step. The DOSY experiment was repeated with diffusion delay periods of (200, 300, and 400) ms.

The diffusion of the TSP signal in m-2-HEAA was determined by DOSY experiments at two diffusion delays of (50 and 10) ms. The DOSY experiment was done with an internal diffusion reference consisting of 300 mg of TSP.

The self-diffusion coefficients were calculated in each DOSY experiment by fitting the intensity of each NMR signal to the following equation:[16]

$$\frac{I(G)}{I(0)} = \mathrm{e}^{-DQ} \tag{1}$$

where $I(G)$ is the signal integral in the presence of the gradient, $I(0)$ is the intensity of the signal with the lowest gradient, D is the self-diffusion coefficient, and Q is the gradient strength, which was calculated according to the following equation:

$$Q = q^2\left(t + \frac{4\delta}{3} + \frac{5\tau_1}{4} + \frac{\tau_2}{4}\right) \tag{2}$$

where t is the diffusion delay used in the experiment and q and the delay variables (δ, τ_1, and τ_2) are explained in the original reference.[16]

Preparation of the ILs. 2-(Methylamino)ethanol was placed in a three-necked flask made entirely of glass and equipped with a reflux condenser, a PT-100 temperature sensor for controlling the temperature, and a dropping funnel. The flask was mounted in a thermostatic bath. The organic acids were added dropwise to the flask under stirring with a magnetic stir bar. The reaction is a simple acid−base neutralization[8] that creates an ester salt of *N*-methyl-2-ethanolamine, which, in a general form, can be expressed as follows:

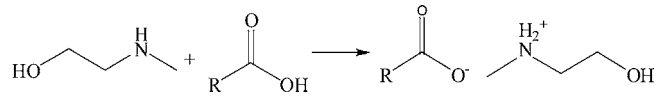

where R is the alkyl group present in the organic acid: formic acid (R = H), acetic acid (R = Me), propionic acid (R = Et), butanoic acid (R = *n*-Pr), isobutanoic acid (R = *i*-Pr), and pentanoic acid (R = *n*-Bu). These chemical reactions are highly exothermic, an adequate control of temperature is essential throughout the chemical reaction; otherwise, heat evolution may produce the dehydration of the salt to the corresponding amide,

as in the case for nylon salts (salts of diamines with dicarboxylic acids). The color varied in each case from transparent to dark-yellow when the reaction process and purification (strong agitation and slight heating for the vaporization of residual nonreacted acid for at least for 48 h) were completed. In order to decrease the water content as much as possible, the IL was dried for 48 h at ambient temperature under a vacuum of 20 kPa with stirring before each use. This time permitted a constant value of the refractive index with respect to drying time to be obtained.

The water content in the ILs was not measured because the room humidity was not completely controlled. In addition, comparisons with standard samples of m-2-HEAA containing H_2O showed a low influence of the humidity on the density. Viscosity was the property most affected by humidity.

Thermodynamic Data Treatment. The measured densities, speeds of sound, and refractive indexes of the ILs were correlated as functions of temperature according to eq 3:

$$Z = A_0 + A_1T + A_2T^2 \tag{3}$$

where Z is the property (density, speed of sound, or refractive index), the A_i are adjustable parameters, and T is the absolute temperature. The apparent viscosity was fitted with an Arrhenius-type equation (normally used for Newtonian fluids), as shown in eq 4:

$$\eta = A_0 e^{A_1/T} \tag{4}$$

where η is the apparent viscosity, T is the absolute temperature, and the A_i are adjustable parameters.

The ions of the IL were considered as a large spherical shapes. Therefore, the effective radius of these molecules can be calculated using the Stokes−Einstein equation for the calculation of the Brownian diffusivity (eq 5), in which the diffusivity D varies directly with absolute temperature and inversely with both viscosity and molecular radius:

$$D = \frac{kT}{r6\pi\eta} \tag{5}$$

where k is the Boltzmann's constant, T is the absolute temperature, η is the viscosity of the medium, and r is the radius of the species.

In order to explore the strength and nature of the interactions between the species of the IL, the molecular radius r was calculated from from the sound velocity and density data as follows:[17]

$$r = \left(\frac{3b}{16\pi N_A}\right)^{1/3} \tag{6}$$

in which N_A is Avogadro's constant and b is given by:

$$b = \frac{M}{\rho} - \left(\frac{RT}{\rho u^2}\right)\cdot\left(\left[1 + \frac{Mu^2}{3RT}\right]^{1/2} - 1\right) \tag{7}$$

where M is the molecular weight, ρ is the density, u is the speed of sound, and R is the gas constant.

Parameter Estimation. The first-approximation parameter estimation for each model was performed using a genetic algorithm code, mMyGA, with a whole-interval search.[18] Next, the resulting fitting parameters were refined using a nonlinear optimization algorithm based on the Marquardt algorithm. Finally, regression was performed with the minimization of the standard deviation between the experimental and calculated values, where the standard deviation (σ) is defined as:

$$\sigma = \left[\sum_{i=1}^{N}\frac{(F_{exptl} - F_{calcd})_i^2}{N}\right]^{1/2} \tag{8}$$

where N is the number of experimental data points and F_{calcd} and F_{exptl} are the property values calculated by the model and obtained from experimental, respectively.

Results and Discussion

The FT-IR and NMR spectra obtained for the ILs studied herein are given in the Supporting Information.

The results of the FT-IR analyses were very similar for all of the ILs. These spectra showed a broad band in the (3500 to 2400) cm^{-1} range that is characteristic of the ammonium structure. The OH stretching vibration is embedded in this band. The broad band centered at 1600 cm^{-1} is a combined band of the carbonyl stretching and N−H plane bending vibrations. Figure 1 displays the FT-IR spectrum of m-2-HEAPr, which shows these bands. The Supporting Information shows the FT-IR spectrum for m-2-HEAF.

NMR spectroscopy provided further insight into the chemical composition of the ILs. The chemical composition was determined by the combination of 1D ^1H, 1D ^{13}C, 1D ^{15}N, 2D TOCSY, 2D HMQC, and 2D HMBC spectra. The 2D experiments provided H−H and H−C through-bond correlations that assisted the NMR signal assignment and confirmed the synthesized structure. For instance, Figure 2 shows the 2D TOCSY spectrum of m-2-HEAPr. The off-diagonal H−H correlation peaks observed in this spectrum correspond to pairs of protons that are connected by covalent bonds to the same molecule and form part of the same coupled spin system. For each IL studied herein, the cation/anion ratio obtained from quantitative analysis of the nonexchangeable signals in the 1D proton spectra (see Figures S1−S6) is ca. 1 ± 0.06, which is in agreement with the expected value for an IL.

Study of the DOSY NMR Spectra. For each ^1H NMR signal, DOSY NMR experiments provided the self-diffusion coefficient of the molecular species to which the signal belonged. Figure 3 shows an example of the analysis of the DOSY diffusion decay curves of m-2-HEAPr at diffusion delays of (200, 300, and 400) ms. This figure shows similar decay curves for the nonexchangeable protons of the same charged component. Nevertheless, there is an unexpected difference between the cation and anion components that is beyond the experimental curve fitting error. Results of the analysis of the DOSY experiments of the other ILs studied herein are given in Table 1 and show that the same situation occurs for the other ILs studied herein, except for m-2-HEAF.

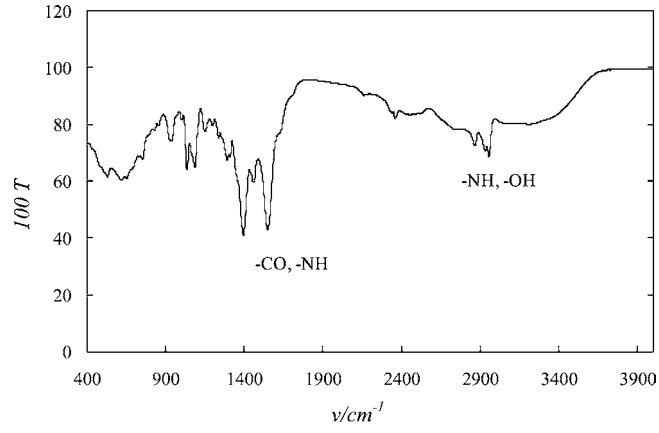

Figure 1. FT-IR spectrum for m-2-HEAPr.

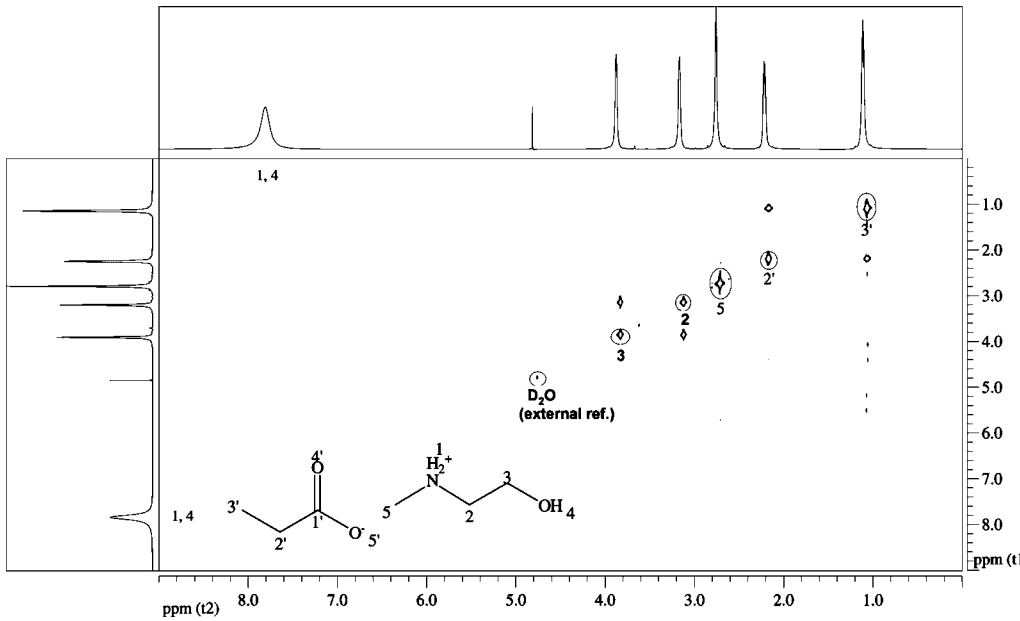

Figure 2. TOCSY spectrum for m-2-HEAPr. The vertical and horizontal traces shown correspond to the 1D proton spectrum. The broad NH_2^+ signal centered at ~7.5 ppm does not appear in the TOCSY spectrum because of its fast transverse relaxation.

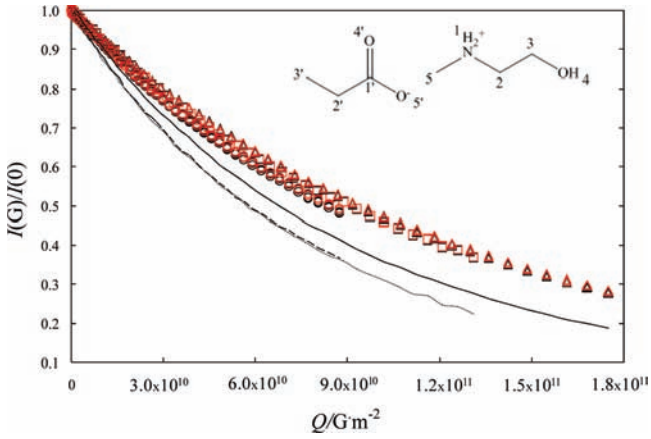

Figure 3. DOSY diffusion decay curves of m-2-HEAPr at three diffusion delays: ○ and dashed line, 200 ms; □ and dotted line, 300 ms; △ and solid line, 400 ms. The symbols are the values for the noninterchangeable species, in black and red for cations and anions, respectively. The lines are the values for the interchangeable species NH_2^+.

Another observation from the diffusion results of Table 1 is that for all of the samples except m-2-HEAF, the diffusion coefficients of the nonexchangeable protons of the ILs in both the cationic and anionic species were affected by the specific diffusion time parameter that was used for the acquisition of the DOSY experiment. In the range of diffusion times studied, from (100 to 400) ms, the trend observed is that the self-diffusion coefficient systematically decreases with increasing diffusion time parameter. We verified that this trend is also present in a sample of m-2-HEAA mixed with 300 μg of TSP as an internal diffusion reference compound. In this case, the diffusion measured for the TSP compound was similarly affected by the diffusion time of the experiment. These observations cannot be explained by the eventual presence of thermal convection in the IL samples,[19] since this effect would increase the diffusion coefficient either with turbulent or constant laminar flux currents, while the observed effect was exactly the opposite. In this regard, the constant laminar flux was already eliminated with the compensated double-stimulated-echo[16] version of the DOSY experiment that was used here.

Table 1. Analysis of the DOSY NMR Spectra Measured for the ILs Studied[a]

t	D^+	D^-	$D^{NH_2^+}$
ms	10^{-12} m^2·s^{-1}	10^{-12} m^2·s^{-1}	10^{-12} m^2·s^{-1}
	N-Methyl-2-hydroxyethylammonium Formate		
0	35.7[b]	57.0[b]	
200	34.90 ± 0.01	55.80 ± 0.03	[c]
300	34.10 ± 0.01	54.60 ± 0.03	[c]
400	34.00 ± 0.01	54.40 ± 0.03	[c]
	N-Methyl-2-hydroxyethylammonium Acetate		
0	7.69[b]	7.94[b]	
200	6.72 ± 0.03	7.02 ± 0.04	9.23 ± 0.08
300	6.01 ± 0.02	6.30 ± 0.02	7.88 ± 0.03
400	5.69 ± 0.02	6.03 ± 0.02	7.86 ± 0.04
	N-Methyl-2-hydroxyethylammonium Propionate		
0	9.39[b]	9.23[b]	
200	8.41 ± 0.02	8.29 ± 0.02	11.8 ± 0.05
300	7.68 ± 0.02	7.65 ± 0.02	11.7 ± 0.06
400	7.36 ± 0.01	7.30 ± 0.02	10.0 ± 0.05
	N-Methyl-2-hydroxyethylammonium Butyrate		
0	10.5[b]	9.64[b]	
200	9.46 ± 0.05	8.66 ± 0.04	20.2 ± 0.01
300	8.66 ± 0.03	7.88 ± 0.03	17.9 ± 0.01
400	8.36 ± 0.03	7.60 ± 0.02	16.5 ± 0.01
	N-Methyl-2-hydroxyethylammonium Isobutyrate		
0	10.8[b]	10.0[b]	
200	9.70 ± 0.03	9.02 ± 0.02	16.8 ± 0.01
300	9.13 ± 0.03	8.43 ± 0.02	14.3 ± 0.01
400	8.59 ± 0.03	7.98 ± 0.02	8.09 ± 0.02
	N-Methyl-2-hydroxyethylammonium Pentanoate		
0	11.2[b]	10.4[b]	
100	10.5 ± 0.02	9.80 ± 0.01	22.7 ± 0.02
200	10.1 ± 0.02	9.37 ± 0.02	19.3 ± 0.01
300	9.28 ± 0.02	8.68 ± 0.02	17.4 ± 0.02

[a] Symbol definitions: t, diffusion time used to encode/decode diffusion in the DOSY experiment; D^+ and D^-, average self-diffusion coefficients of the noninterchangeable signals of the cation and anion, respectively; $D^{NH_2^+}$, apparent diffusion coefficient of the exchangeable proton signal of NH_2^+. The ± values are the uncertainties of the curve fitting. [b] Extrapolated value for 0 ms diffusion time. [c] Signal not detected because of fast relaxation.

The conclusion is that the NMR diffusion results possibly reflect the existence of an aggregation exchange equilibrium in

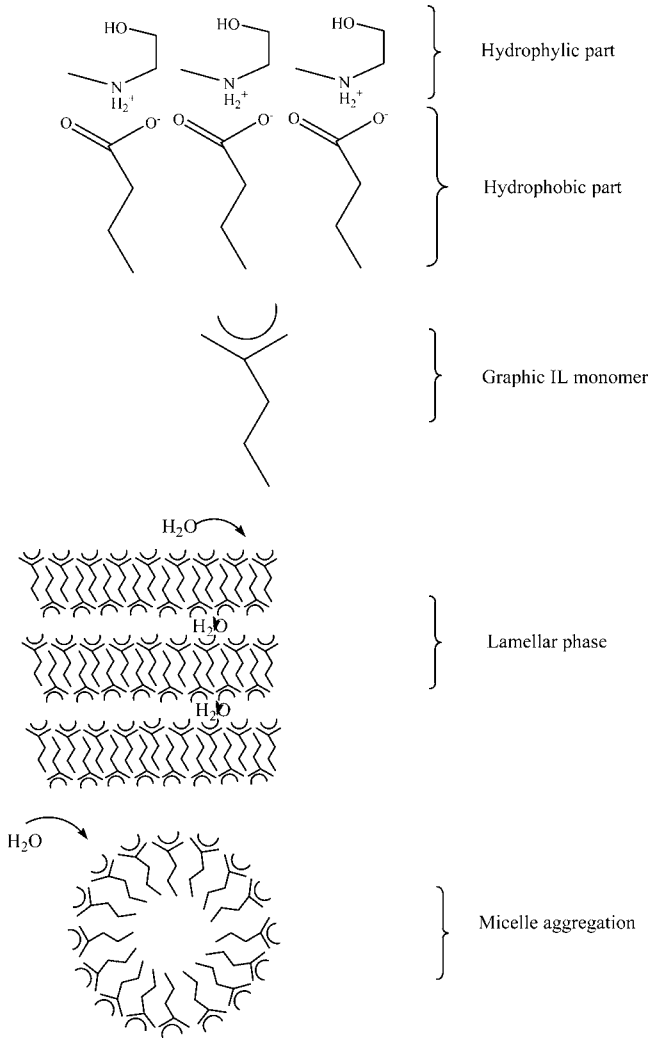

Figure 4. Scheme illustrating the postulated lamellar or micellar liquid-crystal phase of m-2-HEAB.

all of the IL samples except m-2-HEAF. The presence of aggregation is also supported by low-angle X-ray scattering measurements of m-2-HEAB. There is a peak corresponding to aggregates of a size between 9 and 15.5 Å, which is much larger than the optimized molecular modeling of m-2-HEAB in the monomeric state [radius of (3.2 to 3.5) Å]. Moreover, dilution studies recently conducted in our lab have shown the existence of a critical micelle concentration phenomenon in this type of IL (work in preparation).

We speculate that given the amphiphilic nature of these ILs, the alkyl chains of the anion may aggregate to form a lamellar or micellar liquid-crystal phase, as represented in Figure 4. Compartmental diffusion[20,21] occurring in a lamellar/micellar phase would explain the dependence of the diffusion coefficient on the diffusion time in Table 1, including the anomalous case of m-2-HEAF, which lacks the alkyl chain and therefore would not form a lamellar/micellar phase nor exhibit a compartmental diffusion effect.

In the lamellar structure shown Figure 4, the highly hydrophobic alkyl chains of the anion molecules would be packed together in the lamellar/micellar phase, leaving the polar carboxylate anion head groups exposed to the hydrophilic interlamellar/micellar space, in close contact with the cation species and eventually with the water traces. In fact, the formation of lamellar/micellar phases is not uncommon in amphiphilic molecules.[22]

In compartmental systems, the self-diffusion coefficients can be determined by setting a very low diffusion time parameter in the DOSY experiment. However, such an experiment would require special diffusion probes in the spectrometer hardware. A more feasible possibility is to extrapolate the determined self-diffusion coefficients in Table 1 to zero diffusion time, assuming a linear dependence with the diffusion time. Therefore, the self-diffusion coefficients corrected by this method correspond to the authentic diffusion of the species in the compartment.

The corrected values of the diffusion coefficients in Table 1 and the apparent viscosity data in Table 2 can be used to determine the corresponding effective molecular radius of the species by means of the Stokes−Einstein equation (eq 5), which assumes a spherical shape for the molecular entity. However, it was found that the effective radii thus obtained (data not shown) tend to be too small and do not have physical meaning for any of the samples studied except m-2-HEAF, which does not form the lamellar/micellar phase. Clearly, the assumption of spherical shape is not valid for the ILs studied, except in the case of m-2-HEAF.

One important observation from the data in Table 1 is the consistent difference between the diffusion coefficients determined for the cation (D^+) and anion (D^-) for the same sample and same diffusion time. These differences are very remarkable for m-2-HEAF, while for the other ILs the values are relatively more similar. In any case, these differences observed are beyond the experimental fitting error. This behavior is not totally explained by the different compartmental diffusion expected for the cation and anion species in the lamellar/micellar phase, since the m-2-HEAF sample also shows this behavior.

There exists the potential presence of neutral species in the IL mediated by proton exchange reactions (e.g., with the H_2O traces). Thus, the NMR signals of the nonexchangeable protons of one of the components may reflect the combined diffusion of both charged and neutral species that may eventually be different, as the neutral species is in principle the faster one. Therefore, the diffusion coefficients determined with the DOSY experiment and shown in Table 1 could reflect an average of both diffusion coefficients. On this basis, the faster diffusion obtained for the anion than the cation ($D^- > D^+$) in m-2-HEAF in Table 1 probably reflects the presence of relevant mole fraction of neutral formic acid in the sample.

It is also interesting to note from the diffusion coefficients of Table 1 the effect of the length of the alkyl chain. Clearly, the trend observed in these data is that the larger the alkyl chain, the faster is the self-diffusion coefficient of the IL species. This result possibly suggests that the larger the alkyl chain, the larger is the fluidity of the lamellar phase.

A final observation from the data in Table 1 is the diffusion coefficient of the broad signal of NH_2^+ centered at ~7.5 ppm, which is much larger than D^+ and D^- for all of the ILs studied. The diffusion coefficients determined for the NH_2^+ labile protons ($D^{NH_2^+}$) are apparent values, since the signal is affected by fast exchange with other labile protons, in particular with H_2O traces due to inherent sample hygroscopicity and possibly with the OH-4 proton. The detected fast chemical exchange of the NH_2^+ protons is consistent with the exposure of this group to the hydrophilic region in the lamellar/micellar phase model proposed in Figure 4.

Physicochemical Properties. The macroscopic physical properties of the ILs (density, speed of sound, apparent viscosity, and refractive index) were measured, and the results are given in the Supporting Information with the significant figures reported by the device.

Table 2. Molar Mass (M), Experimental Density (ρ), Sound Velocity (u), Refractive Index (n_D), Apparent Viscosity (η), and Molecular Radius (r) Values for the ILs at 298.15 K

	m-2-HEAF	m-2-HEAA	m-2-HEAPr	m-2-HEAB	m-2-HEAiB	m-2-HEAP
M/g·mol^{-1}	121.135	135.162	149.188	163.215	163.215	177.241
ρ/g·cm^{-3}	1.12825	1.10083	1.07127	1.03924	1.04337	1.01621
u/m·s^{-1}	1815.3	1794.8	1690.0	1614.6	1611.3	1548.8
n_D	1.4458[a]	1.4494	1.4534[b]	1.4549	1.4511[c]	1.4538[d]
η/mPa·s	20.27	106.06	215.06	298.15	163.08	234.44
r/Å	2.17	2.27	2.37	2.46	2.46	2.55

[a] T = 298.35 K. [b] T = 298.20 K. [c] T = 298.05 K. [d] T = 298.19 K.

Table 3. Fitting Parameters for Physical Properties and Root-Mean-Square Deviations (σ) in Accordance with Equations 3 and 4 for the Six ILs

	ρ/g·cm^{-1}	u/m·s^{-1}	n_D	η/mPa·s
		N-Methyl-2-hydroxyethylammonium Formate		
A_2	$(2.3341 \pm 0.11) \pm 10^{-7}$	$(6.8704 \pm 0.22) \pm 10^{-4}$	$(8.4066 \pm 4.6) \pm 10^{-7}$	–
A_1	$(-6.9777 \pm 0.066) \pm 10^{-4}$	-2.3677 ± 0.013	$(-7.7232 \pm 2.8) \pm 10^{-4}$	3949.4 ± 80.0
A_0	1.3155 ± 0.001	2460.1 ± 2.1	1.60127 ± 0.043	$(3.7268 \pm 1.0) \pm 10^{-5}$
σ	4.4 ± 10^{-5}	0.1	1.4 ± 10^{-4}	0.6
		N-Methyl-2-hydroxyethylammonium Acetate		
A_2	$(-3.6574 \pm 0.099) \pm 10^{-7}$	$(-1.7489 \pm 0.89) \pm 10^{-4}$	$(-1.5213 \pm 1.7) \pm 10^{-7}$	–
A_1	$(-3.8318 \pm 0.061) \pm 10^{-4}$	-2.4895 ± 0.055	$(-1.5188 \pm 1.0) \pm 10^{-4}$	5541.8 ± 130.0
A_0	1.2476 ± 0.00094	2552.9 ± 8.5	1.5082 ± 0.016	$(9.2245 \pm 4.1) \pm 10^{-7}$
σ	4.2 ± 10^{-5}	0.4	5.4 ± 10^{-5}	3.2
		N-Methyl-2-hydroxyethylammonium Propionate		
A_2	$(-3.9113 \pm 0.096) \pm 10^{-7}$	$(7.8612 \pm 1.0) \pm 10^{-4}$	$(-3.2619 \pm 0.29) \pm 10^{-7}$	–
A_1	$(-4.1827 \pm 0.059) \pm 10^{-4}$	-3.4777 ± 0.062	$(-7.9162 \pm 1.8) \pm 10^{-5}$	5676.0 ± 61.0
A_0	1.2308 ± 0.00091	2657.4 ± 9.6	1.5060 ± 0.0027	$(1.1871 \pm 0.25) \pm 10^{-6}$
σ	4.0 ± 10^{-5}	0.4	9.4 ± 10^{-6}	3.9
		N-Methyl-2-hydroxyethylammonium Butyrate		
A_2	$(-3.5249 \pm 0.090) \pm 10^{-7}$	$(3.2216 \pm 0.14) \pm 10^{-3}$	$(-6.8333 \pm 0.74) \pm 10^{-7}$	–
A_1	$(-4.6411 \pm 0.056) \pm 10^{-4}$	-5.1731 ± 0.086	$(1.1181 \pm 0.45) \pm 10^{-4}$	5848.1 ± 59.0
A_0	1.2090 ± 0.00085	2871.1 ± 13.0	1.4824 ± 0.0069	$(9.2333 \pm 1.8) \pm 10^{-7}$
σ	3.8 ± 10^{-5}	0.6	2.4 ± 10^{-5}	5.2
		N-Methyl-2-hydroxyethylammonium Isobutyrate		
A_2	$(-5.1390 \pm 0.084) \pm 10^{-7}$	$(6.1754 \pm 0.69) \pm 10^{-4}$	$(-4.8174 \pm 2.9) \pm 10^{-7}$	–
A_1	$(-3.3539 \pm 0.052) \pm 10^{-4}$	-3.2309 ± 0.042	$(-1.1006 \pm 18.0) \pm 10^{-5}$	5004.3 ± 65.0
A_0	1.1891 ± 0.00079	2520.0 ± 6.5	1.4971 ± 0.027	$(8.5719 \pm 1.9) \pm 10^{-6}$
σ	3.5 ± 10^{-5}	0.3	9.7 ± 10^{-5}	2.6
		N-Methyl-2-hydroxyethylammonium Pentanoate		
A_2	$(-3.3810 \pm 0.084) \pm 10^{-7}$	$(3.5359 \pm 0.12) \pm 10^{-3}$	$(-3.1521 \pm 3.7) \pm 10^{-7}$	–
A_1	$(-4.7268 \pm 0.052) \pm 10^{-4}$	-5.3202 ± 0.072	$(-1.1653 \pm 2.2) \pm 10^{-4}$	5340.6 ± 64.1
A_0	1.1873 ± 0.00079	2821.1 ± 11.0	1.5166 ± 0.034	$(3.9396 \pm 0.86) \pm 10^{-6}$
σ	3.5 ± 10^{-5}	0.5	1.2 ± 10^{-4}	4.6

The densities and speeds of sound for all of the ILs were studied from (278.15 to 338.15) K with a temperature step of 0.25 K. The viscosity was studied from (288.15 to 323.15) K with a temperature step of 2.5 K for m-2-HEAF, m-2-HEAPr, m-2-HEAB, and m-2-HEAP and 5.0 K for m-2-HEAA and m-2-HEAiB. The range studied for the refractive index was (280 to 323) K with a step of 5.0 K for all of the ILs. These data are provided in the Supporting Information. Table 2 shows the properties at 298.15 K, and Table 3 gives the values of the fitting parameters and the deviations for density, speed of sound, and refractive index (eq 3) and apparent viscosity (eq 4) for all temperatures studied. All but four of the fitting parameter values for the quadratic functions have uncertainties less than the respective parameter values.

For each IL sample, the effective radius r determined from the thermoacoustic data (eq 6) is given in Table 2. As discussed above, all of the studied ILs except m-2-HEAF form a lamellar/micellar phase. Systems forming lamellar/micellar phases do not fulfill the conditions for the applicability of the Stokes−Einstein equation (eq 5), and therefore, the effective radii determined with the thermoacoustic equation and given in Table 2 are likely to be more reliable for these systems. The data in Table 2 show that the effective radius increases with the length of the alkyl chain, with the value being consistent with the sum of the sizes of the cation and anion in the ionic pair.

In Figures 5 to 8, the temperature trends of these physical properties are gathered. The isentropic compressibilities, κ_S, were calculated from the Newton−Laplace equation, and

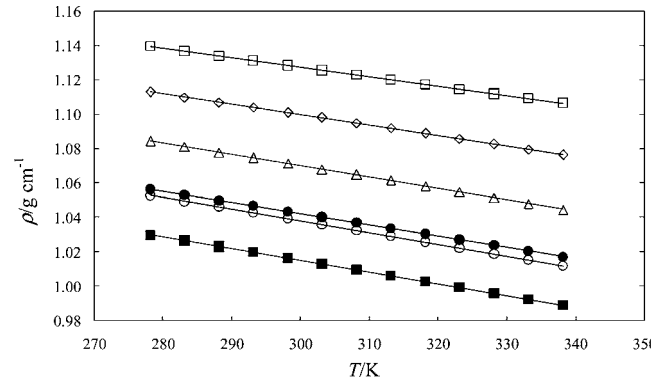

Figure 5. Selected data for the densities of the ILs as functions of temperature: □, m-2-HEAF; ◇, m-2-HEAA; △, m-2-HEAPr; ○, m-2-HEAB; ●, m-2-HEAiB; ■, m-2-HEAP. The solid lines show the corresponding fits to eq 3.

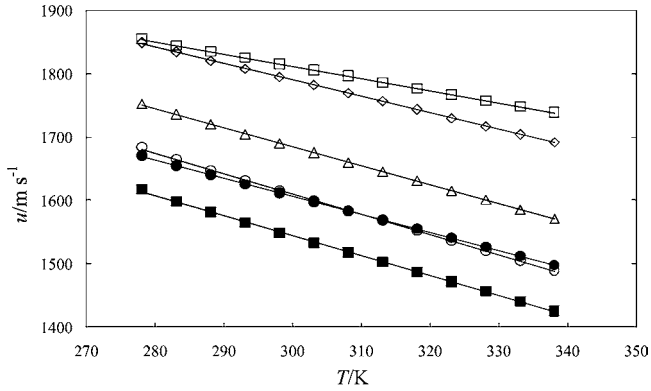

Figure 6. Selected data for the speeds of sound of the ILs as functions of temperature: □, m-2-HEAF; ◇, m-2-HEAA; △, m-2-HEAPr; ○, m-2-HEAB; ●, m-2-HEAiB; ■, m-2-HEAP. The solid lines show the corresponding fits to eq 3.

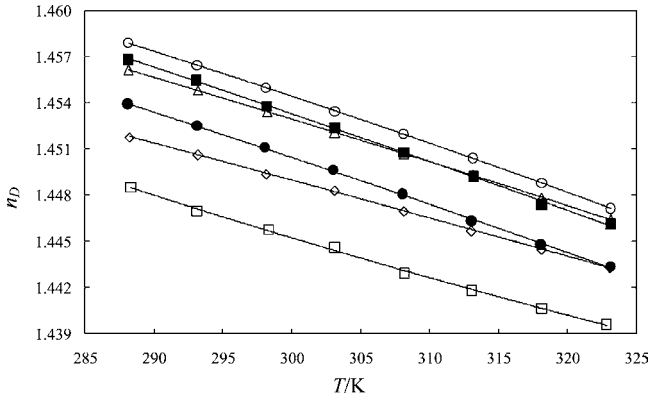

Figure 7. Refractive indexes of the ILs as functions of temperature: □, m-2-HEAF; ◇, m-2-HEAA; △, m-2-HEAPr; ○, m-2-HEAB; ●, m-2-HEAiB; ■, m-2-HEAP. The solid lines show the corresponding fits to eq 3.

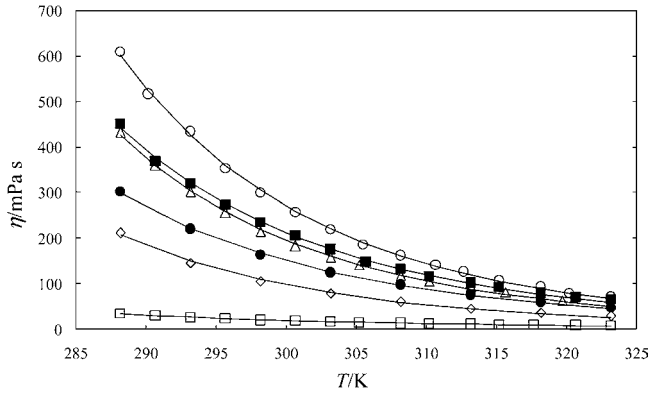

Figure 8. Viscosities of the ILs as functions of temperature: □, m-2-HEAF; ◇, m-2-HEAA; △, m-2-HEAPr; ○, m-2-HEAB; ●, m-2-HEAiB; ■, m-2-HEAP. The solid lines show the corresponding fits to eq 4.

these values for the six ILs are shown in Figure 9. These figures show a decreasing trend in the packing efficiency of the ILs as the molecular weight rises.

The measured apparent viscosities are shown in Figure 8. They exhibit Newtonian behavior, and their values vary exponentially with temperature. In Figure 8, the lowest viscosity corresponds to m-2-HEAF; this IL also shows the largest diffusion coefficient as determined by NMR (Table 1). However, for the other ILs, the NMR diffusion coefficients in Table 1 are relatively similar while the viscosity increases with the length of the alkyl chain (Figure 8). The observation that the enhancement in macroscopic viscosity is unrelated to the NMR diffusion coefficients suggests that the latter do

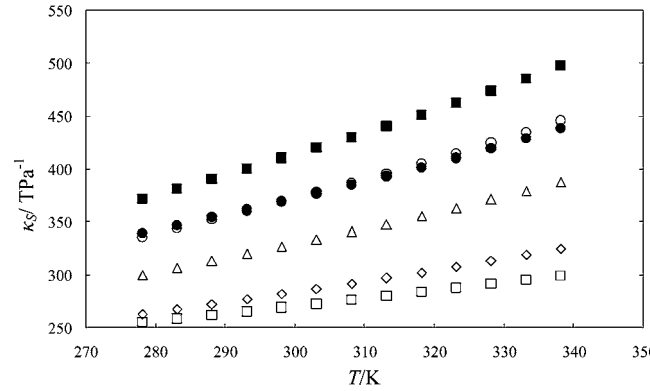

Figure 9. Isentropic compressibilities of the ILs as functions of temperature: □, m-2-HEAF; ◇, m-2-HEAA; △, m-2-HEAPr; ○, m-2-HEAB; ●, m-2-HEAiB; ■, m-2-HEAP.

not reflect the macroscopic diffusion of the IL but just the relatively much faster local or compartmental diffusion in the lamellar/micellar phase, which is in agreement with the nonapplicability of the Stokes−Einstein equation mentioned above.

The apparent viscosities and refractive indexes in Figures 7 and 8 increase with the length of the alkyl chain in the IL. The results for m-2-HEAP were unreliable because of its high hygroscopicity, which affected the measurements (data are shown).

The effect of temperature on the density, speed of sound, refractive index, and apparent viscosity can be seen in Figures 5 to 8. For all of the samples studied, there is an inverse relationship between these properties and the temperature, in agreement with the expectation for fluids.

Conclusions

Six ammonium-based Brønsted acid ILs have been synthesized, and their NMR spectra confirmed the molecular structures.

The diffusion NMR results suggest the existence of an ordered lamellar/micellar liquid-crystal phase for those ILs that contain an alkyl chain in the anion species. For systems forming lamellar/micellar phases, the inherent anisotropy suggests that local structure models should be applied to best explain the macroscopic behavior in terms of the molecular arrangement.

Acknowledgment

The advice from Dr. Bruno Dacuña Mariño (X-ray unit, USC) for suggestions, acquisition, and interpretation of X-ray data is greatly acknowledged.

Supporting Information Available:

Figures S1−S13 and Tables S1−S3. This material is available free of charge via the Internet at http://pubs.acs.org.

Literature Cited

(1) Sheldon, R. Catalytic reactions in ionic liquids. *Chem. Commun.* **2001**, 2399–2407.
(2) Bates, E. D.; Mayton, R. D.; Ntai, I.; Davis, J. H., Jr. CO_2 capture by a task-specific ionic liquid. *J. Am. Chem. Soc.* **2002**, *124*, 926–927.
(3) Huddleston, J. G.; Willauer, H. D.; Swatloski, R. P.; Visser, A. E.; Rogers, R. D. Room temperature ionic liquids as novel media for "clean" liquid−liquid extraction. *Chem. Commun.* **1998**, 1765–1766.
(4) Zhang, S.; Zhang, Q.; Zhang, Z. C. Extractive desulfurization and denitrogenation of fuels using ionic liquids. *Ind. Eng. Chem. Res.* **2004**, *43*, 614–622.

(5) Fuller, J.; Carlin, R. T.; Osteryoung, R. A. The room temperature ionic liquid 1-ethyl-3-methylimidazolium tetrafluoroborate: Electrochemical couples and physical properties. *J. Electrochem. Soc.* **1997**, *144*, 3881–3886.
(6) Marsh, K. N.; Boxall, J. A.; Lichtenthaler, R. Room temperature ionic liquids and their mixtures - A review. *Fluid Phase Equilib.* **2004**, *219*, 93–98.
(7) Kato, R.; Gmehling, J. Activity coefficients at infinite dilution of various solutes in the ionic liquids $[MMIM]^+[CH_3SO_4]^-$, $[MMIM]^+[CH_3OC_2H_4SO_4]^-$, $[MMIM]^+[(CH_3)_2PO_4]^-$, $[C_5H_5NC_2H_5]^+[(CF_3SO_2)_2N]^-$ and $[C_5H_5NH]^+[C_2H_5OC_2H_4OSO_3]^-$. *Fluid Phase Equilib.* **2004**, *226*, 37–44.
(8) Bicak, N. A new ionic liquid: 2-hydroxyethylammonium formate. *J. Mol. Liq.* **2005**, *116*, 15–18.
(9) Greaves, T. L.; Weerawardena, A.; Fong, C.; Krodkiewska, I.; Drummond, C. Protic ionic liquids: solvents with tunable phase behavior and physicochemical properties. *J. Phys. Chem. B* **2006**, *110*, 22479–22487.
(10) Iglesias, M.; Torres, A.; Gonzalez-Olmos, R.; Salvatierra, D. Effect of temperature on mixing thermodynamics of a new ionic liquid: {2-Hydroxyethylammonium formate (2-HEAF) + short hydroxylic solvents}. *J. Chem. Thermodyn.* **2008**, *40*, 119–133.
(11) Cota, I.; Gonzalez-Olmos, R.; Iglesias, M.; Medina, F. New short aliphatic chain ionic liquids: synthesis, physical properties, and catalytic activity in aldol condensations. *J. Phys. Chem. B* **2007**, *111*, 12468–12477.
(12) Iglesias M.; Garcia R.; Gonzalez-Olmos, R.; Salvatierra, D.; Mattedi S. Synthesis and influence of temperature on thermodynamic properties of new ionic liquids. Presented at the 1st International Congress on Green Process Engineering (GPE 2007), Toulouse, France, April 24−26, 2007.
(13) Sierra, J.; Martí, E.; Mengíbar, A.; González-Olmos, R.; Iglesias, M.; Cruañas, R.; Garau, M. A. Effect of new ammonium based ionic liquids on soil microbial activity. Presented at the 5th Society of Environmental Toxicology and Chemistry World Congress, Aug 3−7, 2008, Sydney, Australia.
(14) Giernoth, R.; Bankmann, D.; Schlörer, N. High performance NMR in ionic liquids. *Green Chem.* **2005**, *7*, 279–282.
(15) Cobas, J. C.; Sardina, F. J. Nuclear magnetic resonance data processing. MestRe-C: A software package for desktop computers. *Concepts Magn. Reson.* **2003**, *19A*, 80–96.
(16) Jerschow, A.; Muller, N. Suppression of convection artifacts in Stimulated-Echo Diffusion experiments. Double-Stimulated-Echo experiments. *J. Magn. Reson.* **1997**, *125*, 372–375.
(17) Iloukhani, H.; Rostami, Z. Measurement of some thermodynamic and acoustic properties of binary solutions of *N*,*N*-dimethylformamide with 1-alkanols at 30 °C and comparison with theories. *J. Solution Chem.* **2003**, *32*, 451–462.
(18) Álvarez, V. H.; Larico, R.; Ianos, Y.; Aznar, M. Parameter estimation for VLE calculation by global minimization: Genetic algorithm. *Braz. J. Chem. Eng.* **2008**, *25*, 409–418.
(19) Jerschow, A. Thermal convection currents in NMR flow profiles and implications for coherence pathway selection. *J. Magn. Reson.* **2000**, *145*, 125–131.
(20) Shemesh, N.; Özarslan, E.; Basser, P. J.; Cohen, Y. Measuring small compartmental dimensions with low-*q* angular double-PGSE NMR: The effect of experimental parameters on signal decay. *J. Magn. Reson.* **2009**, *198*, 15–23.
(21) Sen, P. N. Time-dependent diffusion coefficient as a probe of geometry. *Concepts Magn. Reson.* **2004**, *23A*, 1–21.
(22) Burducea, G. Lyotropic liquid crystals I. Specific structures. *Rom. Rep. Phys.* **2004**, *56*, 66–86.

Received for review June 30, 2009. Accepted December 1, 2009. V.H.Á. acknowledges the Movilidade Internacional Santander Scholarship. S.M. is thankful for the financial support for her postdoctoral leave from CNPQ-Brazil. They are also grateful for the support of the *PF&PT* research team at the University of Santiago de Compostela (USC) during their stay there. M.I. is thankful for the support of the Direccion Xeral de Investigacion, Desenvolvemento e Innovacion, Conselleria de Innovación e Industria (Xunta de Galicia, Spain).

JE900550V